Impact of polydispersity on multipolar resonant scattering in emulsions

Benoit Mascaro, Thomas Brunet,[a] Olivier Poncelet, and Christophe Aristégui
Université de Bordeaux, CNRS, UMR 5295, I2M-APy, F-33405 Talence, France

Simon Raffy and Olivier Mondain-Monval
Université de Bordeaux, CNRS, UPR 8641, CRPP, F-33600 Pessac, France

Jacques Leng
Université de Bordeaux, CNRS, Rhodia, UMR 5258, LOF, F-33608 Pessac, France

(Received 6 November 2012; revised 22 January 2013; accepted 28 January 2013)

The influence of size polydispersity on the resonant acoustic properties of dilute emulsions, made of fluorinated-oil droplets, is quantitatively investigated. Ultrasound attenuation and dispersion measurements on various samples with controlled size polydispersities, ranging from 1% to 13%, are found to be in excellent agreement with predictions based on the independent scattering approximation. By relating the particle-size distribution of the synthesized emulsions to the quality factor of the predicted multipolar resonances, the number of observable acoustic resonances is shown to be imposed by the sample polydispersity. These results are briefly discussed into the context of metamaterials for which scattering resonances are central to their effective properties.
 [http://dx.doi.org/10.1121/1.4792140]

PACS number(s): 43.35.Bf, 43.20.Fn, 43.20.Hq [ANN] Pages: 1996–2003

I. INTRODUCTION

Sound scattering by suspensions and emulsions has been studied theoretically and experimentally for many decades[1] and has found various applications in acoustics such as particle sizing.[2–4] Contrary to the long-wavelength regime ($ka \ll 1$) usually considered for the ultrasonic study of particulate mixtures, the resonant scattering regime ($ka \geq 1$) has been the subject of few experimental works due to both the complex effects of the multipolar resonances and the difficulties associated with observing them at high frequencies.

One important difficulty is the achievement of quasi-monodisperse particulate mixtures, which is essential to evidence multipolar resonant features at relatively high ka from a collection of particles in suspension. Indeed, the individual resonances, predicted from the Resonant Scattering Theory for single objects,[5–7] tend to be masked by an averaging process when a polydisperse collection of objects contributes to the scattered field. Since the first experimental works on manufactured millimetric metallic spheres,[8,9] multipolar resonances have been observed in suspensions of calibrated polystyrene microspheres.[10,11] Recently we have reported the achievement of highly monodisperse emulsions made of fluorinated-oil droplets exhibiting a wide collection of multipolar resonances.[12] For polydisperse media, taking into account the measured particle-size distribution (PSD) gives a better macroscopic description of the random media made of solid particles,[13] liquid droplets,[12] or gaseous bubbles.[14]

Contrary to the mean size of particles, it is difficult to control precisely the size polydispersity of the mixture, i.e., the standard deviation of the PSD. This parameter is usually imposed by the experimental setup and cannot be easily adjusted, e.g., for solid particle suspensions.[15] On the other hand, robotics allows the production of liquid droplets with adjustable sizes, providing model systems for experimental studies of the size polydispersity impact on the resonant scattering features.

In this paper, we measure both the effective attenuation coefficients and phase velocities of several emulsions of fluorinated-oil droplets with controlled size polydispersities ranging from 1% to 13%. Samples were intentionally manufactured with a low volume fraction Φ of oil droplets, close to 1% to facilitate the experimental measurements and the theoretical interpretations in the framework of the Independent Scattering Approximation (ISA), which is usually interpreted as a "one-way multiple scattering model."[16] In Sec. II of the paper, the expression for the effective wavenumber (attenuation coefficient and phase velocity) of the coherent pressure wave propagating in a dilute emulsion is derived within the framework of the ISA. The role of the modal amplitudes on the resonant acoustic properties (attenuation peaks and phase-velocity dispersion) is discussed. In Sec. III, we describe both the protocol for achieving emulsions with controlled size polydispersities and the experimental setup used to perform the acoustical measurements. Section IV follows with the comparisons between experimentally determined and theoretically predicted attenuation coefficients and phase velocities for the polydisperse emulsions. At last, we study a bidisperse emulsion viewed as a mixture of two distinct quasi-monodisperse emulsions (bimodal distribution).

II. MODELING OF SIMPLE AND MULTIPLE SCATTERED PRESSURE WAVES

Many theoretical derivations have been proposed concerning wave propagation in media with disordered

[a]Author to whom correspondence should be addressed. Electronic mail: thomas.brunet@u-bordeaux1.fr

 0001-4966/2013/133(4)/1996/8/$30.00

heterogeneities, from the coherent propagation regime (effective medium theories) to the diffusive regime. The wave propagation in such media involves multiple scattering the description of which relies on various assumptions and approximations. We consider the case of low volume fractions of scatterers to minimize multiple scattering interactions and then to focus on the resonances of the individual scatterers. In such case, the thermal waves can be neglected.[3]

Now, the well-known scattering of a plane incident pressure wave by a single spherical fluid inclusion is briefly reminded. In the following, the mass density and the wavenumber of the pressure wave are, respectively, ρ_0, k_0 $(=\omega/v_0+\mathrm{i}\alpha_0)$ in the surrounding medium and ρ_1, k_1 $(=\omega/v_1+\mathrm{i}\alpha_1)$ in the inclusions. Note that v_i and α_i stand for the phase velocity and attenuation coefficient in the medium i (=0 or 1), ω denoting the angular frequency.

For convenience, the time factor $\mathrm{e}^{-\mathrm{i}\omega t}$ will be omitted in the expressions of the following acoustical fields. The pressure field $p_{inc}(r,\theta)\equiv \mathrm{e}^{\mathrm{i}(k_0 r\cos\theta)}$ of the incident wave interacting with a spherical inclusion of radius a can be represented as follows[17]

$$p_{inc}(r,\theta)=\sum_{n=0}^{\infty}\mathrm{i}^n(2n+1)\mathrm{j}_n(k_0r)\mathrm{P}_n(\cos\theta), \tag{1}$$

where j_n is the spherical Bessel function of order n and P_n are the Legendre polynomials. The scattered pressure field p_{sc} and that refracted into the sphere p_r, are expressed in a similar manner by[17]

$$p_{sc}(r,\theta)=\sum_{n=0}^{\infty}\mathrm{i}^n(2n+1)A_n\mathrm{h}_n(k_0r)\mathrm{P}_n(\cos\theta) \tag{2}$$

and

$$p_r(r,\theta)=\sum_{n=0}^{\infty}\mathrm{i}^n(2n+1)B_n\mathrm{j}_n(k_1r)\mathrm{P}_n(\cos\theta), \tag{3}$$

where h_n is the spherical Hankel function of the first kind of order n, A_n, and B_n being the partial wave amplitudes.

Invoking the continuity of both the pressure and the normal displacement at the sphere surface $(r=a)$, leads to a linear system of equations for the amplitudes A_n and B_n. The solutions for the scattered field amplitudes are

$$A_n=-\frac{qj_n'(k_0a)\mathrm{j}_n(k_1a)-\mathrm{j}_n(k_0a)j_n'(k_1a)}{qh_n'(k_0a)\mathrm{j}_n(k_1a)-\mathrm{h}_n(k_0a)j_n'(k_1a)}, \tag{4}$$

with $q=\rho_1k_0/\rho_0k_1$ and where $'$ denotes the derivative with respect to the variable k_0a or k_1a.

Next we consider wave propagation in a medium containing a random distribution of a low volume fraction of identical spheres. The coherent-wave propagation in such media is well described by ISA. In this framework, the effective wavenumber $k_{eff}=\omega/v+\mathrm{i}\alpha$ is given by

$$k_{eff}^2=k_0^2+4\pi\eta F(0) \tag{5}$$

with η the number of inclusions per unit volume and $F(0)$ the forward scattering amplitude given by

$$F(0)\equiv F(0,k_0a,k_1a)=\frac{1}{\mathrm{i}k_0}\sum_{n=0}^{\infty}(2n+1)A_n. \tag{6}$$

Figure 1 shows computations with a fluorinated oil (FC-40, Fluorinert®) for the inclusions ($\rho_1=1.85\,\mathrm{g\ cm^{-3}}$ and $v_1=640\ \mathrm{m\ s^{-1}}$) and with a water-based gel for the matrix ($\rho_0=1\,\mathrm{g\ cm^{-3}}$, $v_0=1492\,\mathrm{m\ s^{-1}}$ at 20 °C, and $\alpha_0=83\times10^{-6}\,\mathrm{mm^{-1}\ MHz^{-2}}$). These two constituents were selected for their high contrast in phase velocity, appropriate to enhance resonant phenomena.[12] The resonance frequencies of the spherical scatterers can be defined from the maxima of the partial wave amplitude moduli $|A_n|$, or from the frequency-variations of the phase angle of the coefficients A_n. The phase jumps from $+\pi$ to $-\pi$ of the phase angle

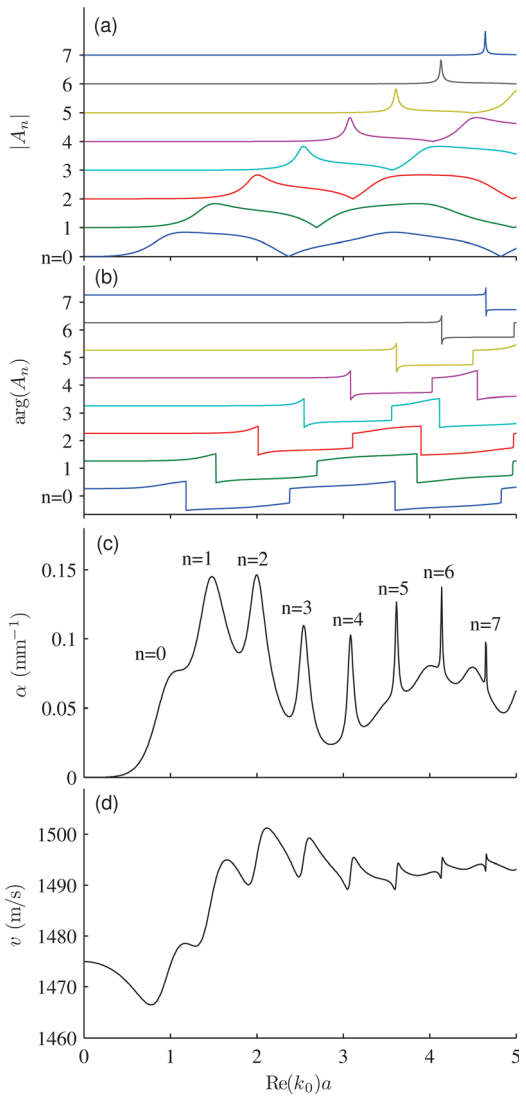

FIG. 1. (Color online) (a) Modulus and (b) phase angle of the modal amplitudes A_n versus the reduced frequency $\mathrm{Re}(k_0)a$, computed for a plane wave scattered away from a single fluid droplet of fluorinated oil suspended in a water-based gel matrix. (c) Effective attenuation coefficient and (d) phase velocity of the coherent pressure wave propagating in a monodisperse emulsion of fluorinated-oil droplets dispersed in water-based gel matrix (ISA). The volume fraction is $\Phi=1\%$.

indicate the resonance frequencies where $|A_n|$ reaches maxima. At these resonances, the wavenumber of the coherent field exhibits attenuation peaks and fast variations of the phase velocity as seen in Fig. 1.

The fundamental acoustic resonances of the monopolar ($n = 0$) and the dipolar ($n = 1$) modes occur within a large frequency domain as illustrated in Fig. 1(a). However, these fundamental resonances become sharper and sharper as n increases, allowing us to define and precisely measure a quality factor $Q_{res} = f_{res}/\Delta f_{res}$ for $n \geq 3$ with the resonance frequency f_{res} of the considered mode n and the full width at half maximum Δf_{res} of the resonance peak observed on the modal amplitude modulus. From Fig. 1(a), the quality factor Q_{res} is equal to 10, 24, 56, and 140 for the fundamental resonance frequencies of the modes $n = 3$, $n = 4$, $n = 5$, and $n = 6$, respectively. Observe that beyond $\mathrm{Re}(k_0)a = 3$, the second harmonic resonances of the modes $n = 0$, 1, 2 also contribute to the attenuation and dispersion along with the fundamental resonances of the modes $n \geq 4$.

In practice, the size polydispersity is responsible for the attenuation peak spreading and tends to smooth the sharpest peaks predicted for monodisperse systems at high frequencies.[12,13] Beyond a certain frequency, it is essential to take into account the particle-size distribution to describe precisely the resonant features of real media, i.e., polydisperse systems. In the context of ISA, the effective wavenumber for a polydisperse medium is then given by[14]

$$k_{eff}^2 = k_0^2 + \int_a 4\pi\eta(a)F(0, k_0 a, k_1 a)\mathrm{d}a \tag{7}$$

with $\eta(a)$ the particle-size distribution and $\Phi = \int_a \eta(a) \times (4\pi a^3/3)\mathrm{d}a$ the total volume fraction of particles. In this study, we deal with Gaussian distributions $\eta(a) = (\mathrm{N}/\sqrt{2\pi}\sigma) \times \mathrm{e}^{-[(a-\bar{a})^2/2\sigma^2]}$ for the PSD, where σ is the standard deviation, $\bar{a}$ is the mean radius, and $\mathrm{N} = \int_a \eta(a)\mathrm{d}a$ is the total number of particles per unit volume. Finally, the size polydispersity of the medium is defined as $\sigma/\bar{a}$. Note that the latter parameter can also be viewed as a quality factor $Q_{PSD} = \bar{a}/\sigma$, characterizing the narrowness of the PSD.

III. SYNTHESIS AND EXPERIMENTAL CHARACTERIZATION OF POLYDISPERSE EMULSIONS

A. Control of the size polydispersity

As recently reported,[12] we achieved calibrated emulsions made of pure fluorinated-oil droplets (FC-40, Fluorinert®) suspended in an aqueous gel-matrix (Carbopol® ETD 2050, 0.2 wt. %) by using robotics. Such Bingham fluid, owing a low yield stress (≈10 Pa), behaves like water in the megahertz range we investigated, i.e., no shear waves can propagate. By injecting the oil within the gel-matrix at constant flow rate ($Q \approx 20\,\mu$l/min), *via* a syringe moving at constant velocity ($V \approx 100$ mm/s), regularly spaced spherical droplets are produced in rows with an excellent reproducibility of size. Because the size of the droplets depends only on the ratio Q/V, their radius is accurately controlled by tuning the syringe velocity V during the injection of the fluorinated oil at constant flow rate Q. As illustrated in Fig. 2(a), the faster the syringe moves, the smaller the droplets. Then a specific PSD is obtained by mixing different rows of droplets as shown in Fig. 2(b).

The particle-size distribution of each sample was characterized afterward by optical microscopy on about a hundred droplets. Their mean radius $\bar{a}$ was bounded by 100 and 200 μm. The PSD standard deviation σ ranged from 1 to 10 μm providing size polydispersities $\sigma/\bar{a}$ ranging from 1% to 13% [see Fig. 4(a)]. Thus we are able to produce highly monodisperse emulsions as well as emulsions with accurately controlled size-distributions. The volume fractions Φ of droplets are estimated from the fluorinated oil quantity injected into the gel matrix and are about 1% in all the experiments.

B. Ultrasound spectroscopy

The acoustic parameters of the samples are identified by using an ultrasonic spectroscopy technique based on backward signals from a water-immersed plastic cell[18] the walls of which are parallel to the face of the emitter/receiver transducer. The plastic cell (p) is made of weakly lossy PMMA ($\rho_p = 1.19\,\mathrm{g/cm^3}$, $v_p = 2670\,\mathrm{m/s}$, and $\alpha_p = 0.0108\,\mathrm{mm^{-1}\,MHz^{-1}}$). It is successively filled with water (w) taken as a reference medium ($\rho_w = 1\,\mathrm{g/cm^3}$, $v_w = 1488\,\mathrm{m/s}$) and with the emulsion (e). With this method, the propagation path length is $2d$.

As shown in Fig. 3, several backward reflected waveforms are collected for the determination of the acoustic properties of the sample. One set of three reference signals is collected with the water-filled cell. Their frequency spectra are given by

$$A = A_0 \mathrm{e}^{-\mathrm{i}\omega t}\mathrm{e}^{\mathrm{i}k_w 2L}R_{wp},$$

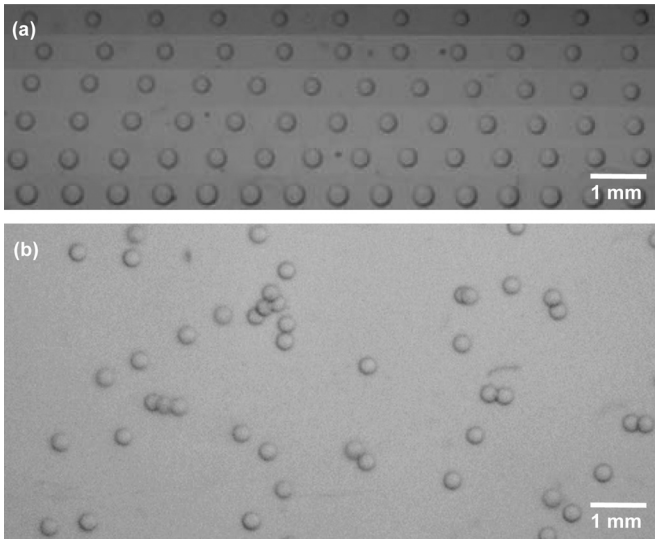

FIG. 2. (a) Rows of perfectly spherical oil-droplets with different radii, synthesized by means of robotics. All droplets were produced at the same oil-flow rate ($Q = 20\,\mu$l/min) by varying the displacement velocity V of the injecting syringe ($V = 72$, 61, 49, 38, 25, and 14 mm/s, from top to bottom). (b) Example of a (random) emulsion obtained after mixing several droplets rows of different sizes. Here, the mean radius $\bar{a}$ of the emulsion is 170 μm, the size polydispersity $\sigma/\bar{a}$ is 5% and the volume fraction Φ is 1%.

$$B = A_0 e^{-i\omega t} e^{ik_w 2L} T_{wp} e^{ik_p 2h} T_{pw} R_{pw},$$

$$C = A_0 e^{-i\omega t} e^{ik_w 2L} T_{wp}^2 e^{ik_p 2h} e^{ik_w 2d} R_{wp} T_{pw}^2,$$

where R_{ij} and T_{ij} (with $i, j = w$ or p) stand for the wave amplitude reflection and transmission coefficients at the interface between the media i and j when the ultrasonic wave is incident from medium i to medium j. The wavenumbers k_w and k_p govern the wave propagation in water and PMMA, respectively.

Next the reference liquid (water) is removed, and the cell is filled with the emulsion and replaced at its initial position in the water tank. Then a second set of signals is collected. Their frequency spectra are defined as

$$\tilde{A} = A,$$

$$\tilde{B} = A_0 e^{-i\omega t} e^{ik_w 2L} T_{wp} e^{ik_p 2h} T_{pw} R_{pe},$$

$$\tilde{C} = A_0 e^{-i\omega t} e^{ik_w 2L} T_{wp} T_{pe} e^{ik_p 2h} e^{ik_{eff} 2d} R_{ep} T_{ep} T_{pw}.$$

Recalling that $R_{ep} = -R_{pe}$ and $T_{pe}T_{ep} = 1 - R_{pe}^2$,

$$\frac{\tilde{C}}{\tilde{B}} = e^{ik_{eff} 2d}(R_{pe}^2 - 1). \tag{8}$$

The reflection coefficient R_{pe} is evaluated from the ratio $\tilde{B}/B = R_{pe}/R_{pw}$, where the coefficient R_{pw} is determined from the mass densities and the longitudinal phase velocities of the cell walls and of water.

The attenuation coefficient α of the emulsion is then deduced from the modulus of Eq. (8),

$$\alpha = -\frac{1}{2d} \ln \left| \frac{1}{(R_{pe}^2 - 1)} \frac{\tilde{C}}{\tilde{B}} \right|, \tag{9}$$

where d is deduced from the reference measurements performed in water

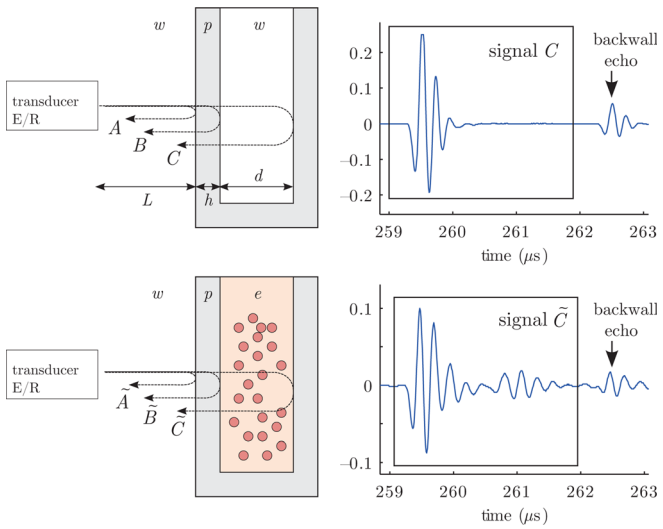

FIG. 3. (Color online) Schematic diagram of the experimental set-up for the ultrasonic characterization of emulsions from appropriate backward reflected signals. The PMMA cell (p) immersed in water (w) is filled either with (top) water (w) or (bottom) with the emulsion (e) to be characterized.

$$d = \frac{v_w}{2\omega}[\arg(R_{pw}^2 - 1) - \Delta\theta_w], \tag{10}$$

with $\Delta\theta_w = \arg(C) - \arg(B)$ denoting phase differences between the spectra C and B.

The phase velocity v is obtained from the phase angles of the complex-valued terms involved in Eq. (8),

$$v = v_w \frac{\Delta\theta_w - \arg(R_{pw}^2 - 1)}{\Delta\theta_e - \arg(R_{pe}^2 - 1)}, \tag{11}$$

with $\Delta\theta_e = \arg(\tilde{C}) - \arg(\tilde{B})$.

The incident wave is a broadband pulse generated by a transducer of central frequency 5 MHz and of 1-in. diameter. The cell-wall thickness ($h = 5$ mm) and the cell depth ($d = 8$ mm) have been chosen to clearly distinguish in the time domain the set of three echoes represented in Fig. 3. The propagation path length is also long enough to measure accurately the attenuation coefficient α of the tested medium.[19] Because the acoustic waves are multiply scattered by the droplets in the emulsions, both the coherent and incoherent parts coexist. The spatial averaging of the acoustic field over the transducer surface reduces the incoherent part. Under this condition, the coherent part is accessible without averaging on various configurations of the disorder.

To evaluate the contribution of the incoherent part, one can compare the total propagation distance $2d$ to the elastic mean free path ℓ_e, which is related to the effective attenuation coefficient by $\ell_e = 1/2\alpha$. In this paper, only the coherent regime occurs because the ratio $\ell_e/2d$ ensures the incoherent part to be very low. Over the frequency range [0–10 MHz], the highest value of the effective attenuation measured in the samples is $\alpha_{max} \approx 0.15$ mm^{-1}. Because the least elastic mean free path is about 3 mm, the total wave propagation path length $2d$ corresponds to at most five mean free paths ℓ_e. Finally, for the considered dilute emulsions, the experimental setup leads to the coherent wave measurement. This has been experimentally verified by a good matching between a single waveform and the averaged waveform.

IV. RESULTS AND DISCUSSION

A. Polydisperse emulsions

Samples have been made with several size polydispersities $\sigma/\bar{a}$ ranging from 1% to 13% with a droplet distribution following a Gaussian function as mentioned in Sec. II. The experimental measurements of the attenuation coefficient α and phase velocity v for each sample are displayed versus the reduced frequency in Fig. 4. The mean radius $\bar{a}$ of the oil droplets dispersed in each sample being not identical, the representation versus the reduced frequency $\mathrm{Re}(k_0)\,\bar{a}$ is the most appropriate one for a direct comparison of the results between the different emulsions. By using an inversion technique based on a least squares optimization (detailed in the Appendix), a best fit procedure permits the evaluation of the three parameters characterizing a Gaussian PSD: The mean radius $\bar{a}$, the size polydispersity $\sigma/\bar{a}$, and the volume fraction Φ from the acoustic measurements. Those parameters determined by optical microscopy and

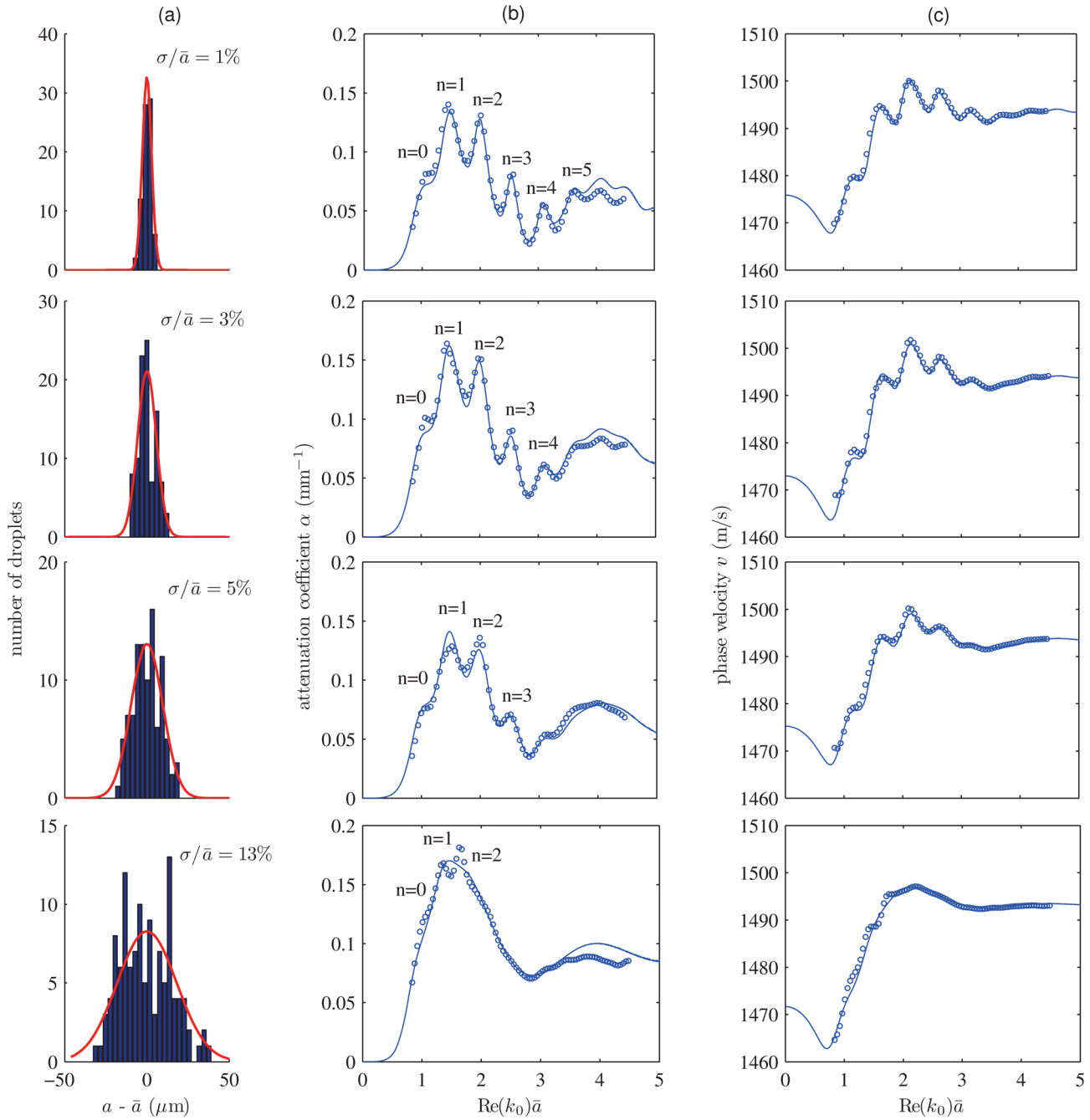

FIG. 4. (Color online) Optical and acoustical measurements performed on emulsions with an increasing polydispersity. (a) Centered droplet-radius histograms obtained from optical microscopy with their fitted Gaussian distributions (—). (b) Attenuation coefficient and (c) phase velocity versus the reduced frequency Re(k_0) $\bar{a}$: Acoustical measurements (○) and their best fit (—) obtained with the inversion procedure detailed in the appendix.

acoustical measurements have been found to be very close (see Table I). In particular, the size polydispersities of the emulsions are well recovered by acoustical measurements. Thus ultrasonic spectroscopy carried out in the resonant regime could provide an accurate method of polydisperse particle size characterization for systems of diverse acoustic contrast, usually studied in the long wavelength regime.[20]

Figure 4 also shows that the scattering resonant features progressively disappear as the size polydispersity increases. For example, the attenuation peaks are clearly observable until the mode order $n = 5$ for the 1%-polydisperse emulsion

TABLE I. Comparison between the optical microscopy measurement and the acoustical identification, of the Gaussian size-distribution parameters for four samples of fluorinated-oil droplet emulsions. Φ was determined from the quantity of oil injected into the gel matrix.

Sample (Number)	$\bar{a}_{opt}$ (μm)	$(\sigma/\bar{a})_{opt}$ (%)	Φ (%)	$\bar{a}_{ac}$ (μm)	$(\sigma/\bar{a})_{ac}$ (%)	Φ_{ac} (%)
1	185	1.4	≈1	181	2.41	0.95
2	174	3.1	≈1	173	3.60	1.10
3	172	4.9	≈1	170	4.82	0.98
4	128	12.7	≈1	142	13.4	1.19

TABLE II. Summary of observable (√) or non-observable (×) fundamental acoustic resonances of several modes ($3 \leq n \leq 6$) occurring in fluorinated-oil droplet emulsions with different size polydispersities $\sigma/\bar{a}$ ranging from 1% to 13%. For comparison, the quality factor Q_{res} of these resonances (determined from Fig. 1) is mentioned for each mode as well as the inverse of the size polydispersity $Q_{PSD} = \bar{a}/\sigma$, which characterizes the particle-size distribution of the samples.

	$n = 3$ $Q_{res} = 10$	$n = 4$ $Q_{res} = 24$	$n = 5$ $Q_{res} = 56$	$n = 6$ $Q_{res} = 140$
$\sigma/\bar{a} = 1\%$ $Q_{PSD} = 100$	√	√	√	×
$\sigma/\bar{a} = 3\%$ $Q_{PSD} = 33$	√	√	×	×
$\sigma/\bar{a} = 5\%$ $Q_{PSD} = 20$	√	×	×	×
$\sigma/\bar{a} = 13\%$ $Q_{PSD} = 7.5$	×	×	×	×

(sample 1) while the fundamental resonances of the first three modes ($n = 0$, 1, 2) are hardly identifiable for a 13%-polydisperse emulsion (sample 4).

Table II makes an inventory of the observable (√) or non observable (×) attenuation peaks for each sample. As mentioned in Sec. II, these attenuation peaks are due to the resonances of the individual droplets the resonant behavior of which can be viewed through their modal amplitudes A_n. The narrowness of the resonance peaks [Fig. 1(a)] is characterized by the quality factor Q_{res} the values of which are reminded in Table II. By introducing $Q_{PSD} = \bar{a}/\sigma$ associated with the droplet-size distribution and corresponding to the inverse of the size polydispersity, the two parameters Q_{res} and Q_{PSD} can be quantitatively compared for all resonances occurring in each sample. Table II shows then that Q_{PSD} must be higher than Q_{res} to clearly observe a distinguishable attenuation peak. Any oil-droplet emulsion, of which Q_{PSD} is lower than the quality factor Q_{res}, does not exhibit any prominent features in their attenuation and phase velocity spectra.

TABLE III. The same as Table I but for the bidisperse emulsion considered in Fig. 5.

	$\bar{a}_{opt}$ (μm)	$(\sigma/\bar{a})_{opt}$ (%)	Φ (%)	$\bar{a}_{ac}$ (μm)	$(\sigma/\bar{a})_{ac}$ (%)	Φ_{ac} (%)
Size 1	151	2.5	0.5	150	2.18	0.5
Size 2	179	1.7	0.7	177	1.42	0.75

B. Bidisperse emulsions

A bimodal emulsion was synthesized by mixing two distinct quasi-monodisperse droplet distributions the mean radii of which are $\bar{a}_1 = 150$ μm and $\bar{a}_2 = 180$ μm, respectively. The present bidisperse sample has been made with a targeted total volume fraction Φ ($=\Phi_1 + \Phi_2$) of fluorinated oil of about 1%. The volume fraction $\Phi_2 = 0.7\%$ has been taken slightly higher than the volume fraction $\Phi_1 = 0.5\%$ to have the same numbers of droplets per unit volume for each quasi-monodisperse distribution, i.e., $\Phi_1 \bar{a}_2^3 = \Phi_2 \bar{a}_1^3$.

The experimental results for the acoustic properties of the bidisperse emulsion are shown versus the frequency f in Fig. 5. In spite of the non-linear form of Eq. (7), the total attenuation results from the simple addition of the contributions of each quasi-monodisperse distribution, owing to the low absorption of the pure matrix ($\alpha_0 \ll (\omega/v_0)$) and the low volume fraction of droplets (about 1%) as mentioned in a previous study.[12] Thus we observe that the simultaneous exhibition of the resonant features of each distribution leads to smooth spectra or enhanced resonance features, depending on the phase agreement between the response of each distribution. At low frequency, the resonant response is smoothed out, while sharp attenuation peaks remain around 4 and 5 MHz. These types of resonant effect combinations can then be used to design structures exhibiting specific properties over a given spectral domain.

As done for polydisperse emulsions, the mean sizes $\bar{a}_1$ and $\bar{a}_2$, the size polydispersities $\sigma_1/\bar{a}_1$ and $\sigma_2/\bar{a}_2$, and the volume fractions Φ_1 and Φ_2 of each distribution are

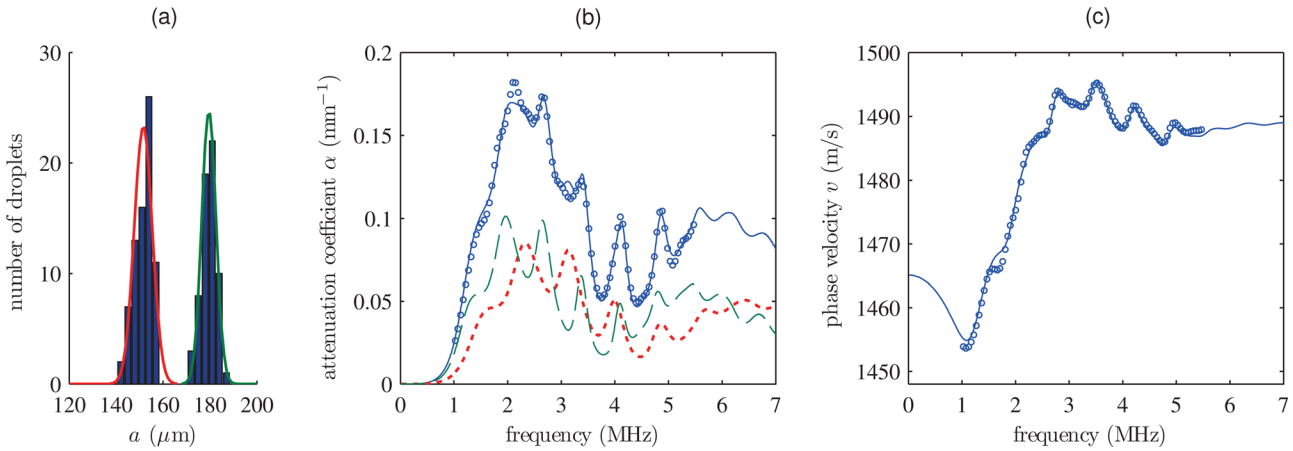

FIG. 5. (Color online) The same as Fig. 4 but for the bimodal emulsion. The predicted attenuation coefficients for each quasi-monodisperse droplet distributions shown in (a) have been also displayed in (b) (dotted line for $\bar{a}_1 = 151$ μm, and dashed line for $\bar{a}_2 = 179$ μm). Computations have been performed by using the acoustic parameters reported in Table III.

recovered all at once from the attenuation spectrum, only. Characteristics obtained from the optical microscopy and from the acoustic measurements are in excellent agreement as illustrated in Table III.

V. CONCLUSION

This work provides experimental results on the way that collective resonances observed in the resonant scattering regime ($ka \geq 1$) are affected by the particle-size distribution of a random media, especially by their size polydispersity. Robotics allow the fast production of emulsions with well-controlled droplet-size distributions, which exhibit clear resonant features (attenuation peaks and variations of the phase velocity). From the coherent wave propagation analysis, we evidenced and quantified experimentally that the higher the polydispersity, the lower the number of observable resonant modes. We quantitatively related the quality factor Q_{res} of each multipolar resonance mode to the size polydispersity $\sigma/\bar{a}$, demonstrating that the control of the latter parameter is crucial to hope to observe resonant features in locally resonant materials. As an example to confirm such allegation, it has been reported that a standard deviation of about $\sigma = \pm$ 6% cancels metamaterial features for microwaves such as negative bands exhibited by a magnetic metamaterial made of split-ring resonators fabricated with varying amounts of disorder.[21]

ACKNOWLEDGMENTS

This work was supported by EOARD (Grant FA8655-11-M-4006), by Agence Nationale pour la Recherche (Grant 2011-BS0902101), and by Conseil Régional d'Aquitaine.

APPENDIX: INVERSION PROCEDURE

The identification of the droplet-size distribution and the droplet volume-fraction is performed from the measured attenuation $\alpha_{exp}(f)$, only. The droplet mean-radius $\bar{a}$ depends on the frequency location of the attenuation peak maxima, while the size polydispersity ratio is related to the wave damping. A small change in droplet radius induces a substantial change in the frequency location of peaks, while the volume fraction of droplets is linked to the attenuation coefficient by a linear dependence for low concentrations.[12]

The theoretical attenuation $\alpha_{th}(\bar{a}, \sigma, \Phi, f)$ is determined from Eq. (7) for different values of the mean radius $\bar{a}$, the standard deviation σ, and the total volume fraction Φ for a droplet-size Gaussian distribution. The minimization of the objective function over the frequency range $[f_1–f_2] = [1–5\ \text{MHz}]$

$$\sum_{f_i=f_1}^{f_2} \{\alpha_{exp}(f_i) - \alpha_{th}(\bar{a}, \sigma, \Phi, f_i)\}^2 \tag{A1}$$

by using the Nelder–Mead simplex optimization algorithm gives the optimal parameters $\bar{a}_{ac}$, σ_{ac}, and Φ_{ac}, which leads to the best matching between the theoretical and measured wave attenuations.

In the special case of the bimodal distribution defined by the superimposition of two Gaussian distributions (with the parameters $\bar{a}_j$, σ_j, and Φ_j, $j = 1, 2$), the attenuation coefficient α depends on six parameters. The objective function to be minimized becomes

$$\sum_{f_i=f_1}^{f_2} \{\alpha_{exp}(f_i) - \alpha_{th}(\bar{a}_1, \sigma_1, \Phi_1, \bar{a}_2, \sigma_2, \Phi_2, f_i)\}^2. \tag{A2}$$

The properties of the matrix and the inclusions being *a priori* known, we investigate here the effect of their variation on the minimization result. While the mass density is usually measured with a good accuracy, phase velocity uncertainty of few meters per second can be induced by temperature variation or by a wrong propagation path length. The conducted parametric study showed that only the phase velocity v_1 in the inclusions affects substantially the frequency location of the resonance peaks, and then the identification of the mean radius $\bar{a}$, through the product $k_1 a$ arising in Eq. (7). Let us underline that the volume fraction Φ and size polydispersity $\sigma/\bar{a}$ are not impacted by the variation of the phase velocity v_1 and that the phase velocity v_0 in the gel matrix does not affect the three parameters $\bar{a}$, σ, and Φ. Thus the reliability of the inversion procedure is not sensitive to a slight variation of the matrix properties.

[1] J. R. Allegra and S. A. Hawley, "Attenuation of sound in suspensions and emulsions: Theory and experiments," J. Acoust. Soc. Am. **51**, 1545–1564 (1972).
[2] F. Alba, G. Crawley, J. Fatkin, D. Higgs, and P. Kippax, "Acoustic spectroscopy as a technique for the particle sizing of high concentration colloids, emulsions and suspensions," Colloids Surf., A **153**, 495–502 (1999).
[3] R. E. Challis, M. J. W. Povey, M. L. Mather, and A. K. Holmes. "Ultrasound techniques for characterizing colloidal dispersions," Rep. Prog. Phys. **68**, 1541–1637 (2005).
[4] A. S. Dukhin and P. J. Goetz, *Ultrasound for Characterizing Colloids—Particle Sizing, Zeta Potential, Rheology* (Elsevier, Amsterdam, 2002), pp. 1–372.
[5] L. Flax, L. R. Dragonette, and H. Überall, "Theory of elastic resonance excitation by sound scattering," J. Acoust. Soc. Am. **63**, 723–731 (1978).
[6] K. A. Sage, J. George, and H. Überall, "Multipole resonances in sound scattering from gas bubbles in a liquid," J. Acoust. Soc. Am. **65**, 1413–1422 (1979).
[7] M. F. Werby, H. Überall, A. Nagl, S. H. Brown, and J. W. Dickey, "Bistatic scattering and identification of the resonances of elastic spheroids," J. Acoust. Soc. Am. **84**, 1425–1436 (1988).
[8] L. R. Dragonette, R. H. Vogt, L. Flax, and W. G. Neubauer. "Acoustic reflection from elastic spheres and rigid spheres and spheroids. II. Transient analysis," J. Acoust. Soc. Am. **55**, 1130–1137 (1974).
[9] W. G. Neubauer, R. H. Vogt, and L. R. Dragonette, "Acoustic reflection from elastic spheres. I. Steady-state signals," J. Acoust. Soc. Am. **55**, 1123–1129 (1974).
[10] A. E. Hay and A. S. Schaafsma, "Resonance scattering in suspensions," J. Acoust. Soc. Am. **85**, 1124–1138 (1989).
[11] J. Mobley, K. R. Waters, C. S. Hall, J. N. Marsh, M. S. Hughes, G. H. Brandenburger, and J. G. Miller, "Measurements and predictions of the phase velocity and attenuation coefficient in suspensions of elastic microspheres," J. Acoust. Soc. Am. **106**, 652–659 (1999).
[12] T. Brunet, S. Raffy, B. Mascaro, J. Leng, R. Wunenburger, O. Mondain-Monval, O. Poncelet, and C. Aristégui, "Sharp acoustic multipolar-resonances in highly monodisperse emulsions," Appl. Phys. Lett. **101**, 011913 (2012).
[13] I. Alig and D. Lellinger, "Frequency dependence of ultrasonic velocity and attenuation in two-phase composite systems with spherical scatterers," J. Appl. Phys. **72**, 5565–5570 (1992).
[14] V. Leroy, A. Strybulevych, J. H. Page, and M. G. Scanlon, "Sound velocity and attenuation in bubbly gels measured by transmission experiments," J. Acoust. Soc. Am. **123**, 1931–1940 (2008).
[15] C. S. Hall, J. N. Marsh, M. S. Hughes, J. Mobley, K. D. Wallace, J. G. Miller, and G. H. Brandenburger, "Broadband measurements of the

attenuation coefficient and backscatter coefficient for suspensions: A potential calibration tool," J. Acoust. Soc. Am. **101**, 1162–1171 (1997).
[16]Z. Ye and L. Ding, "Acoustic dispersion and attenuation relations in bubbly mixture," J. Acoust. Soc. Am. **98**, 1629–1636 (1995).
[17]J. J. Faran, "Sound scattering by solid cylinders and spheres," J. Acoust. Soc. Am. **23**, 405–418 (1951).
[18]T. Norisuye, S. Sasa, K. Takeda, M. Kohyama, and Q. Tran-Cong-Miyata, "Simultaneous evaluation of ultrasound velocity, attenuation and density of polymer solutions observed by multi-echo ultrasound spectroscopy," Ultrasonics **51**, 215–222 (2011).
[19]A. N. Kalashnikov and R. E. Challis, "Errors and uncertainties in the measurement of ultrasonic wave attenuation and phase velocity," IEEE Trans. Ultrason. Ferroelectr. Freq. Control **52**, 1754–1768 (2005).
[20]A. Richter, F. Babick, and S. Ripperger, "Polydisperse particle size characterization by ultrasonic attenuation spectroscopy for systems of diverse acoustic contrast in the large particle limit," J. Acoust. Soc. Am. **118**, 1394–1405 (2005).
[21]J. Gollub, T. Hand, S. Sajuyigbe, S. Mendonca, S. Cummer, and D. R. Smith, "Characterizing the effects of disorder in metamaterial structures," Appl. Phys. Lett. **91**, 162907 (2007).